Polarization-Sensitive Nanowire Photodetectors Based on Solution-Synthesized CdSe Quantum-Wire Solids

Amol Singh,[†] Xiangyang Li,[§] Vladimir Protasenko,[‡] Gabor Galantai,[‡] Masaru Kuno,[‡] Huili (Grace) Xing,[†] and Debdeep Jena*,[†]

Department of Electrical Engineering, University of Notre Dame, Notre Dame, Indiana 46556, Department of Chemistry and Biochemistry, University of Notre Dame, Notre Dame, Indiana 46556, and Shanghai Institute of Technical Physics, Chinese Academy of Sciences, Shanghai, China 200083

Received June 1, 2007; Revised Manuscript Received July 30, 2007

ABSTRACT

Polarization-sensitive photodetectors are demonstrated using solution-synthesized CdSe nanowire (NW) solids. Photocurrent action spectra taken with a tunable white light source match the solution linear absorption spectra of the NWs, showing that the NW network is responsible for the device photoconductivity. Temperature-dependent transport measurements reveal that carriers responsible for the dark current through the nanowire solids are thermally excited across CdSe band gap. The NWs are aligned using dielectrophoresis between prepatterned electrodes using conventional optical photolithography. The photocurrent through the NW solid is found to be polarization-sensitive, consistent with complementary absorption (emission) measurements of both single wires and their ensembles. The range of solution-processed semiconducting NW materials, their facile synthesis, ease of device fabrication, and compatibility with a variety of substrates make them attractive for potential nanoscale polarization-sensitive photodetectors.

Introduction. Growing interest exists in exploiting the unique optical and electrical properties of nanostructures, such as nanocrystal quantum dots (QDs) and metallic or semiconducting nanotubes and nanowires (NWs).[1,2] As opposed to solids made of close-packed 0D materials, 1D nanostructures are materials of the lowest dimensionality that allow the simultaneous exploitation of size-quantization effects as well as efficient carrier band transport. Furthermore, when integrated with most underlying substrates, bottom up 1D nanostructures have been shown to retain their native optical and electrical properties.[3−6] This contrasts to epitaxially grown nanostructures, where lattice matching constraints restrict the materials that can be integrated together, preventing a more thorough exploration of the optical and electrical properties of epitaxially grown heterostructures. As a consequence, bottom up systems exhibit great flexibility that can be exploited for novel nanoscale device applications.

The primary growth technique for electronic grade 1D nanowires has, to date, been based on vapor−liquid−solid (VLS) growth.[7,8] However, a number of more recent solution-based chemical syntheses have emerged, providing alternative routes to high-quality 1D nanostructures. They include supercritical-fluid−liquid−solid (SFLS)[9] as well as solution−liquid−solid (SLS) growth.[10] These solution-based approaches exhibit a number of potential advantages over chemical vapor deposition (CVD)-based techniques such as VLS. They include low cost, potential synthetic scalability, chemically and electronically passivated NW surfaces, solubility in various solvents, and compatibility with a variety of substrates. Resulting 1D nanowires are highly crystalline and are optically and/or electrically active as evidenced by recent studies focusing on their optical and electrical properties.[9]

At the same time, nanocrystal quantum dots have also been made using analogous solution chemistry.[11−13] They and their close packed assemblies possess many of the same advantages as solution-synthesized NWs. Of particular relevance to the current study, photoconductivity has been demonstrated using closed-packed QD "solids".[14−18] Although photon

* Corresponding author. E-mail: Djena@nd.edu.
† Department of Electrical Engineering, University of Notre Dame.
‡ Department of Chemistry and Biochemistry and Notre Dame Radiation Laboratory, University of Notre Dame.
§ Chinese Academy of Sciences.

absorption and electron−hole pair generation in these systems is generally efficient,[19−22] carrier extraction is often difficult because the process involves hopping transport between QDs prior to collection at the electrodes, compounded by Coulomb blockade effects.[23] This also represents a potential problem for practical applications of carrier multiplication effects recently observed in single nanocrystal QDs.[24,25] As a consequence, transport inefficiencies have begun to be addressed, in part, by thermal and/or chemical treatments of QD solids to reduce their insulating nature. To illustrate, nanocrystal solids have been heat treated to remove excess surfactant on individual nanoparticle surfaces.[18] Close packed solids have also been exposed to short chain organics such as butylamine to effectively reduce their interdot spacing. This has led to dramatic improvements in carrier transport, allowing the development of a variety of nanocrystal devices such as photodetectors and field effect transistors (FETs).[26]

In this work, we demonstrate polarization-sensitive photoconductive (PC) photodetectors based on solution-synthesized nanowire networks, or "quantum-wire solids". Although considerable effort has gone into making above-mentioned nanocrystal QD photodetectors using bottom up[13,14,26] or top-down methodologies,[27] a number of reasons exist for why complementary NW-based devices may have decided advantages. Among them is the efficient extraction of photogenerated carriers, due to the intrinsic 1D geometry of the material. Furthermore, NW absorption cross sections are nearly 4−5 orders of magnitude larger than that of comparable QDs.[28,29] This will result in much higher photocurrents and improve the responsivity of the photodetectors. Band transport of photogenerated carriers also occurs along the longitudinal nanowire axes, with occasional hopping between wires for random networks, eliminating the need for electron or hole transporting polymers generally used in QD devices. As a consequence, NW photodetectors should exhibit greater external conversion efficiencies because they circumvent the large RC delays intrinsic to variable range hopping and Coulomb blockade effects in QD solids.[23,30] Finally, both dielectric contrast effects as well as size quantization-induced selection rules impart natural polarization sensitivity to the material.[4,31−33] This is an attractive feature not readily achieved with traditional bulk materials and corresponding devices.

More subtle reasons for favoring NW-based photodetectors include the time scale for intraband carrier relaxation. Specifically, intraband relaxation in nanocrystal QDs occurs much faster than in NWs. For example, measured P to S state relaxation rates in CdSe nanocrystals range from 400 fs to 1 ps.[34] This has been observed despite the presence of potential phonon bottleneck effects that could significantly inhibit carrier cooling.[35] In the case of CdSe NWs, intraband relaxation to the band edge occurs within ∼3 ps.[36] This is significantly longer than in the case of complementary QDs or even quantum rods (∼1 ps).[37] Similar behavior has been observed with recently developed CdTe NWs where analogous intraband relaxation occurs within 1 ps.[38] These relatively slow hot-carrier cooling rates imply that NW

photodetectors may be intrinsically more efficient than their QD counterparts simply because photogenerated carriers have more time to be swept out to the electrodes before they relax to the band-edge (upon which they can recombine either radiatively or nonradiatively, leading to a reduction in the photocurrent).

In what follows we present preliminary results on solution-synthesized CdSe quantum-wire solid photodetectors. Temperature-dependent electrical conductivity measurements present evidence for band transport through the quantum-wire solid. Photocurrent action spectra of the solution-processed quantum-wire solids are presented. Action spectra follow the solution linear absorption of the wires, showing that they are responsible for the photoconductivity. Bias-dependent and excitation power-dependent behavior of NW photodetectors is also studied. NW alignment is achieved using dielectrophoresis (DEP) of the wires between pre-existing electrodes made using optical photolithography. Polarization sensitivity of aligned NW photodetectors is demonstrated, making solution-synthesized NW solids highly attractive for facile fabrication of such desirable devices.

Results and Discussion. *Growth/Characterization/Fabrication.* Solution-based CdSe NWs are synthesized using recently developed SLS growth methodologies.[10,39] The general approach uses low-melting nanoparticle (NP) catalysts to promote 1D crystallization in the presence of mild coordinating surfactants such as trioctylphosphine oxide (TOPO). In the current study, low-melting bimetallic Au/Bi core/shell NPs are used as catalysts. Particle sizes range from 1.5 to 3 nm (diameter). More details about their synthesis can be found in ref 39. The NPs are then introduced along with a common selenium precursor, TOP−Se, into a TOPO-based reaction mixture containing ligand-coordinated metal ions. CdO and octanoic acid are used as the metal source and metal coordinating ligand respectively. A rapid color change from clear to dark brown/black occurs when the catalyst and Se precursor are introduced into the CdO solution at high temperatures ($T \sim 330$ °C). This indicates the formation of CdSe NWs. The product is kept heated for approximately 1 min before being cooled to room temperature. Toluene is then added to prevent TOPO from solidifying and an excess of methanol or other polar solvent such as ethanol or isopropanol is added to precipitate the wires. The suspension is then centrifuged to recover a NW precipitate, which is "washed" several more times by repeated suspension and precipitation from toluene using methanol. More details about the synthesis and workup can be found in ref 40. The NWs are subsequently resuspended in either toluene or chloroform. This approach for making nanowires is general and has been used to make other II−VI (CdTe[38]), IV−VI (PbSe[41]), and III−V (InP and GaAs) NWs.

The resulting CdSe NWs are highly crystalline and have diameters in the range of 8−10 nm, below twice the corresponding bulk exciton Bohr radius ($a_B \sim 5.6$ nm). NW interwire diameter distributions range from 25 to 30% and intrawire distributions are on the order of 5%. Figure 1a shows representative high-resolution TEM images of the
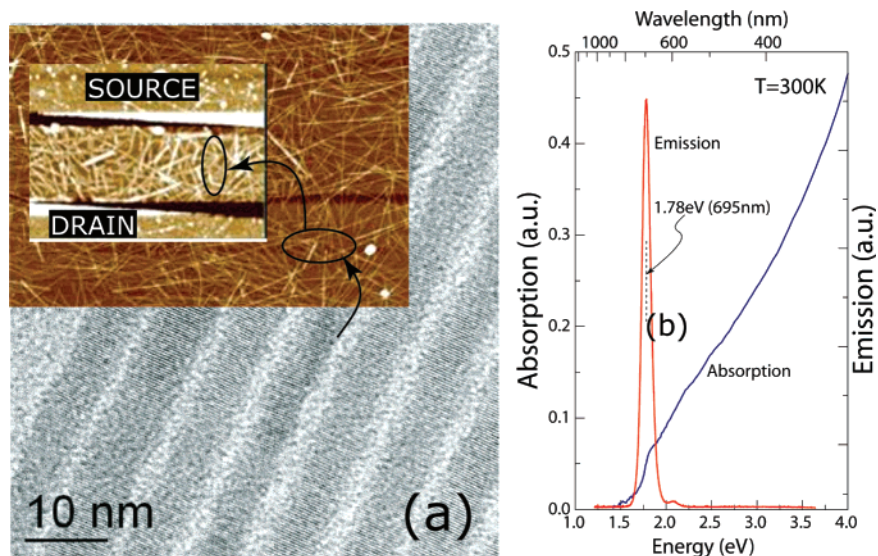
Figure 1. (a) TEM image of solution-synthesized CdSe NWs, with (inset) an AFM image of a network of such NWs formed on a SiO_2/Si substrate. (b) Absorption/emission spectra of the NW ensemble in solution.

wires, illustrating their crystallinity and uniformity. Detailed TEM-based structural analyses indicate that the wires exhibit zinc blende (ZB) and wurtzite (WZ) phase mixtures as well as twinning within ZB sections.[42] Wires grow along the ⟨111⟩ and ⟨0001⟩ directions of the ZB and WZ phases, respectively. Organic surfactants such as TOPO used in the synthesis passivate the NW surface and prevent them from touching/ aggregating. They also provide solubility in common organic solvents and help suppress any potential surface oxidation.

The solution absorption and emission spectrum of a typical CdSe NW ensemble is shown in Figure 1b. A blue shift relative to the bulk band gap of CdSe ($E_g = 1.74$ eV, 300 K) is seen. Structure is also observed at higher energies, suggesting the presence of confinement-induced subbands. This is supported by recent transient differential absorption experiments on CdSe NWs, which reveal at least three features underlying the solution linear absorption spectrum.[36] Band edge emission is also seen with no sign of deep trap emission, both at the ensemble and single wire levels. The absorption cross section of solution-synthesized CdSe NWs has been estimated for regions far to the blue of the band edge. The expression utilized assumes a bulk-like density of states at high energies and is further angle-averaged to account for the random orientation of NWs in solution. This approach has previously been used to model the absorption cross section of nanocrystal QDs and leads to order of magnitude values consistent with those measured experimentally.[29] When the approximation is applied to solution-synthesized CdSe NWs, absorption cross sections of $\sigma \sim 1 \times 10^{-12}$ cm^2 are obtained at the band edge ($\sim$1.75 eV, 1 μm long, $\sim$10 nm diameter).[29] Likewise, values of $\sigma \sim 1 \times 10^{-11}$ cm^2 and $\sigma \sim 2 \times 10^{-11}$ are evaluated at 488 nm (2.54 eV) and 387 nm (3.20 eV), respectively. More recent experimental values, obtained through correlated absorption, transmission electron microscopy, and inductively coupled plasma atomic emission spectroscopy, agree well with these numbers. These values and associated molar extinction

coefficients are nearly 5 orders of magnitude larger than that of comparable diameter nanocrystal QDs.[29]

Transport in CdSe Quantum-Wire Solids. Quantum-wire solids are formed by drop-casting these solution-synthesized CdSe NWs onto glass, or SiO_2/Si substrates. The NWs form a dense connected, yet conductive random network. This is illustrated by the inset of Figure 1a showing an atomic force microscope (AFM) image of the channel between two electrodes. The density of the NW network and overall conductivity of the device can be significantly enhanced by repeated drop casting. This allows relatively thick, highly absorbing, NW layers to be formed in a facile manner. Metal−quantum-wire solid−metal photodetector structures are fabricated with drain-source separation $L_{ds} = 30\ \mu$m using shadow-masking and metal deposition. Gold is used as the electrode material and thermal annealing in a Forming gas (95% N_2, 5% H_2) atmosphere for 1 min at 300 °C enables contacts that permit ohmic current flow under optical illumination. Using a global back gate, we have demonstrated in an earlier work that the conductivity of these quantum-wire networks can be capacitively modulated by more than 4 orders of magnitude at room temperature, verifying their semiconducting nature.[43] In essence, the quantum-wire solid formed out of the nanowire network should possess many properties of a thin film semiconductor, with one crucial difference: optical properties and possibly transport properties should be strongly affected by the inherently one-dimensional nature of the active regions.

Ideal characteristics of nanoscale photodetectors include low dark currents, large induced photocurrents, low resistivity under illumination, and high on/off ratios. Figure 2a shows typical current−voltage characteristics from the NW photodetectors under dark, and under white light illumination ($I = 540$ mW/cm^2, wavelength averaged). The NW photodetectors exhibit very low dark currents ($\sim$10s of pA at $V_{DS} = 5$ V), indicating that few free carriers exist in the nanowires at room temperature. At room temperature, the
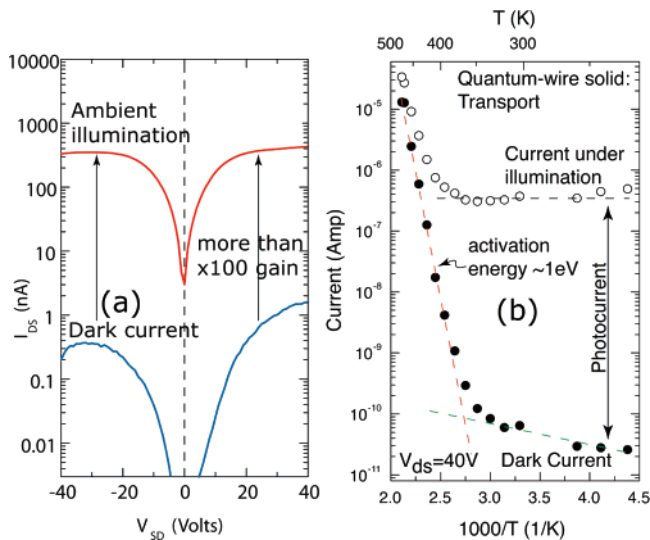
Figure 2. (a) $I–V$ curve of a quantum-wire solid showing the current in dark and under illumination, showing strong photoconductivity. (b) Currents in dark and under broadband illumination at 40 V bias as a function of temperature (different device from Figure 2a). A sharp thermal activation onset is observed, indicating that carriers that are thermally generated across the band gap of CdSe dominate the transport properties.

low density of carriers in the NW limits the dark current. This becomes evident when the current−voltage measurement is performed for a range of temperatures (Figure 2b). The dark current increases with temperature, and for $T >$ 360 K, a very sharp increase in current with activation energy of $E_A \sim 1$ eV is observed. The dark current changes by 5 orders of magnitude in the temperature range 360 K < T < 470 K. This temperature dependence is explained by assuming that the current through the quantum-wire solid occurs by band transport, and the current density $J \propto n_{total}v_{dr}$, where v_{dr} is the drift velocity of carriers, $n_{total} = n_{thermal} + n_{optical}$ and $n_{thermal} = N_{D0} \exp(-E_D/k_BT) + n_i$ is the total density of mobile electrons in the conduction band (a) due to contributions from the residual donors of density N_{D0} with activation energy E_D and (b) due to intrinsic electrons thermally excited across the band gap. Here, $n_i = \sqrt{N_C N_V} \exp(-E_g/2k_BT)$, where N_C and N_V are the effective density of states at the conduction and valence band edges. Assuming that the dark current is predominantly due to thermally generated carriers and that the drift velocity does not change considerably over the temperature range considered, the temperature dependence of dark current ($J_{dark} \propto n_{thermal}v_{dr}$) is entirely due to its dependence on the total carrier density. Under these approximations, values of $E_g \sim 2$ eV, $N_{D0} \sim 10^2$ cm^{-3}, and $E_D \sim 10$ meV can explain the temperature variation. Typical values of the residual impurity incorporation in the purest semiconductors grown by CVD or other epitaxial techniques are of the order of $N_{D0} \geq 10^{10}$ cm^{-3}, far higher than the solution-processed quantum-wire solid. The extremely low residual impurity incorporation results in extremely low dark currents, which is crucial for the high sensitivity of photodetectors. The interesting thermal behavior demands a more detailed evaluation of transport properties in a later work. It corroborates current understanding that there exists a natural

bottleneck for dopant impurity incorporation during solution growth of semiconductor nanocrystals and nanowires. The band gap energy extracted from the temperature-dependent conductivity exceeds the measured optical band gap by ∼0.22 eV, which is attributed to nonideal ohmic contacts, the assumption of a temperature-independent drift velocity, and the possible effects of the dielectric environment. Though the exact reason for this discrepancy is not clear and is currently being investigated, it does not play a large role in the rest of this work.

Under white light illumination, the current increases by orders of magnitude at room temperature with a corresponding drop of the resistance. The total current now has an additional contribution from photogenerated carriers n_{opt}. From Figure 2b, for $T \leq 360$ K, $n_{opt} \gg n_{thermal}$, but for $T \geq$ 400 K, thermally generated carriers exceed those that are optically generated. These observations indicate the strong intrinsic photoconductivity of quantum-wire solids at ambient temperatures ($T \leq 360$ K) and their potential use as in extremely sensitive photodetectors.

Photocurrent Spectroscopy. The spectroscopic photoresponse of the solution-synthesized CdSe quantum-wire solid is measured by illuminating it using a QTH (quartz−tungsten−halogen) lamp coupled to a Spectra Physics Cornerstone 260 1/4 m monochromator, with a chopper operating at 17 Hz. The effective spot size on the CdSe NW photodetector was 1 mm × 30 μm, the latter is the drain-source spacing. Thin gold wires were bonded to the large metal pads of the photodetectors and connected to a 40 V Agilent E3611A dc power supply and a 1 MΩ resistor/diode biasing circuit in series. The photocurrent was measured from the voltage drop across the bias resistor by locking into the chopper frequency using a SR830 100 kHz DSP lock-in amplifier. A Si photodetector connected to a Merlin Oriel digital lock-in radiometry system was used to calibrate the power spectrum of the QTH lamp. The spectral range of the whole setup (except the Si photodetector used for calibration) covers energies between ∼1 and ∼4 eV (1100−300 nm) with a nominal spectral bandwidth of 0.1 nm. All measurements were performed at room temperature.

The directly measured photocurrent spectrum at a drain-source bias of 10 V is shown in Figure 3a for a device on glass. The photocurrent edge is nearly identical to the absorption edge of the same nanowires measured in solution, as shown in the same figure. A sharp turn-on is observed at 1.79 eV (693 nm), slightly higher than the known fundamental band gap of bulk CdSe ($E_G = 1.74$ eV). Deep states in the band gap have been reported earlier in the literature, observed by photocurrent measurements performed on VLS-grown ZnO nanowires.[44] However, no photocurrent is observed for the solution-processed CdSe wires at photon energies smaller than 1.5 eV, indicating a low concentration of such defects. This is possibly due to the passivation of dangling bonds on the NW surface by organic ligands in the SLS growth process.

When the same measurement was repeated on CdSe quantum-wire solids drop-cast on Si/SiO$_2$ substrates, the photocurrent was observed to oscillate periodically with the
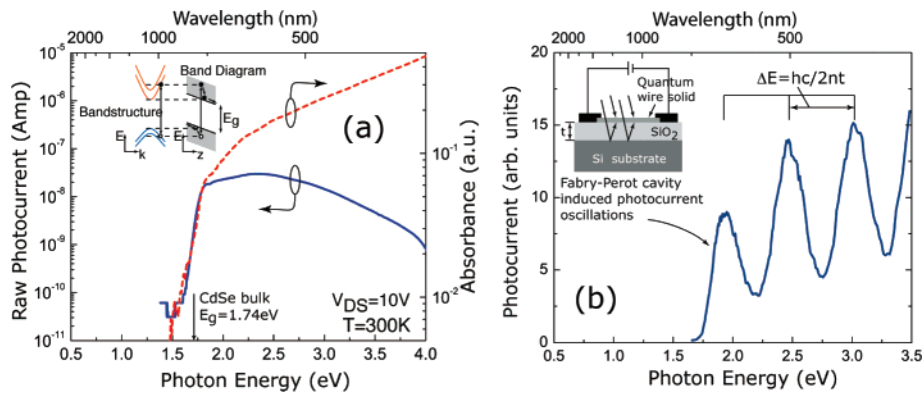
Figure 3. (a) Measured photocurrent spectrum of a random CdSe NW network on a glass substrate superposed on the absorption spectrum. The sharp turn-on of the photocurrent at the band-edge is in close agreement with the absorption spectrum. The inset shows photocarrier generation and transport in the NWs schematically. (b) Similar NW network on SiO₂/Si substrate exhibits oscillations in photocurrent due to multiple reflections of incident photons from the Fabry−Perot etalon formed between the NW surface and the SiO₂/Si interface.

incident photon energy, as shown in Figure 3b. The thickness of the SiO₂ layer is $t_{ox} = 740$ nm. The photocurrent oscillations are due to the Fabry−Perot etalon formed by the NW solid−SiO₂ and the SiO₂−Si interfaces. The separation of peaks in energy for such an etalon, given by $E_{n+1} - E_n = \Delta E = hc/2n_{ox}t_{ox}$, where h is Planck's constant, c is the speed of light in vacuum, and $n_{ox} = 1.46$ is the refractive index of SiO₂, evaluates to ~0.58 eV. The peak separation measured (~0.56 eV) corresponds to this known oxide thickness. This observation implies that resonant-cavity effects can be exploited for photodetectors based on such quantum-wire solids for enhancing the sensitivity to certain wavelengths, and to reject unwanted ones, a feature that has been exploited over the past decade for enhancing the quantum efficiency of epitaxially grown heterostructure photodetectors and resonant-cavity light-emitting diodes (RCLEDs).[45]

Photodetector Responsivity. The responsivity of the CdSe quantum-wire solid photodetector is measured in the following way. The photocurrent spectra are first measured for a range of bias voltages and incident power densities. The measured photocurrent is found to depend on the incident power according to the power law $I_{pc} = A(\lambda) \cdot P_{inc}^{0.8}$ for the entire range of incident power intensities used (here P_{inc} is the incident power); this is consistent with earlier observations.[46] $A(\lambda)$ is a wavelength-dependent coefficient that is experimentally determined. Because the lamp power spectrum is nonuniform over the wavelength regime investigated, it is necessary to scale the photocurrent using the power-law dependence found. This gives us the true photocurrent I_{pc}^{wl} for an effective white light source of uniform power density. The responsivity of a photodetector, defined as $R_\lambda = I_{pc}^{wl}/P_{inc}$ (in A/W units), is equivalent to $R_\lambda = (\eta q/h\upsilon) \cdot G$, where η is the quantum efficiency of the quantum-wire solid, q is the electron charge, and $h\upsilon$ is the incident photon energy. $G = \tau_n/\tau_{tr}$ is the photoconductive gain in the semiconductor, where τ_n and τ_{tr} are the minority carrier lifetime and the transit time across the device, respectively.

The measured responsivity is shown in Figure 4 for a range of bias voltages for a uniform illumination of $P_{inc} = 100$ nW over the photodetector area. The responsivity rejection
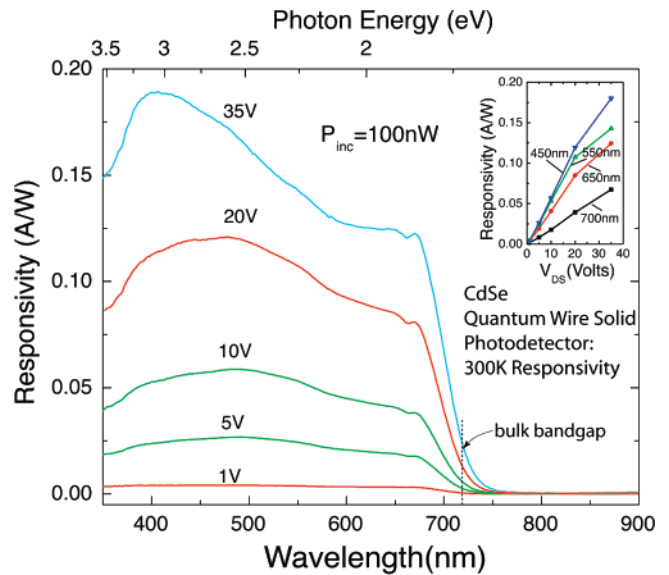

Figure 4. Measured responsivity for drain-source biases changing from 1 to 35 V at 300 K exhibiting a cutoff wavelength close to the bulk CdSe band gap. The inset shows that the responsivity increases linearly with applied bias voltage (and hence the applied electric field) for various wavelengths, indicating that the photoconductive gain is limited by transit time of carriers in the linear drift mobility regime.

ratio between $\lambda = 600$ nm and $\lambda = 800$ nm is found to be ~300 at all applied voltages. From the Fabry−Perot oscillations in Figure 3(b), one can conclude that the quantum-wire solid layer is much thinner than the optical absorption length of CdSe for the range of wavelengths used. In typical bulk photoconductive detectors, increased absorption near the surface and nonradiative recombination at the surface states dominates, resulting in a responsivity that decays as the wavelength decreases. In spite of the fact that the nanowires are extremely thin with large surface to volume ratios, the responsivity observed does not drop till the photon energy reaches ~2.8 eV (450 nm). This feature can be attributed to the surface passivation after the solution synthesis, an advantage of the SLS growth technique. The inset in Figure 4 shows that the responsivity increases linearly with the applied bias voltage. This can be understood from
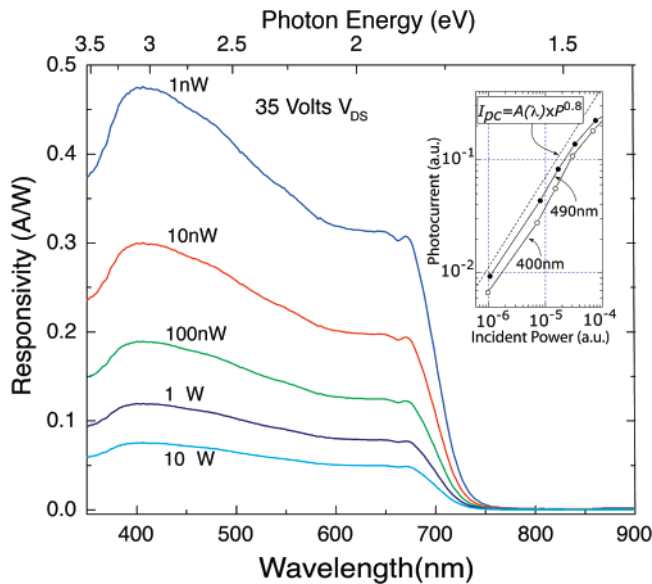
Figure 5. Dependence of the photodetector responsivity at 35 V bias on the incident power. The inset shows the power-law dependence of the measured photocurrent on the incident power.

Figure 6. Polarization-sensitive photocurrent is observed for an aligned CdSe quantum-wire solid (red filled circles). The photo-current measured in a commercial Si photodetector is shown (blue filled circles) for comparison. The solid line is a sinusoid, showing that the photocurrent has a period of π. The DEP technique used for alignment of the NWs is schematically shown in the inset. The isnet in the bottom right corner is an optical image of nanowires aligned between two electrodes.

the dependence of responsivity on the photoconductive gain in the CdSe quantum-wire solid. Assuming that minority-carrier lifetime is constant, gain depends on the transit time of carriers. If the carriers are moving in the drift-mobility regime, the transit time is given by $\tau_{tr} = L/v_{dr} = L^2/\mu_n V_{ds}$, where L is the source-drain separation and μ_n is the electron mobility. If one assumes a reasonable value of mobility of 50 cm^2/(V s), the transit time at 10 V bias would be $\sim$0.2 ns. If the minority carrier lifetime is larger than this value, there would be internal gain. However, if the electric field is high enough to ensure that the fast moving carriers (electrons) are moving at their saturation velocities, $\tau_{tr} = L/v_{sat.}$ independent of the bias voltage. Under such conditions, the internal photoconductive gain would approach a constant value. Thus, the responsivity vs V_{ds} plot should resemble the velocity-field curve for the semiconductor. From the inset of Figure 4, the responsivity increases linearly with the applied bias, and hence it is clear that the carriers move in the drift-mobility regime and not in the saturation velocity regime for the voltage range used.

Precise evaluation of the intrinsic photoconductive gain requires knowledge of the minority carrier lifetime and the mobility. Because these properties of CdSe nanowires are yet to be measured accurately, evaluation of such quantities is not attempted here. For comparison purposes, in the limit of unity quantum efficiency and unity gain (clearly not the situation here), the ideal responsivity should be $R_\lambda(\eta=1,G=1) = \lambda$ (μm)/1.24, which is $\sim$0.3 A/W at 400 nm excitation. The measured responsivity is $\sim$0.17A/W at 35 V bias at that wavelength.

Figure 5 shows the dependence of the responsivity on the excitation power intensity for the detector biased at 35 V. The inset shows the measured power-law dependence of the photocurrent on the excitation intensity. The photodetector sensitivity increases at low incident power due to the sublinear dependence on excitation, which is indeed an
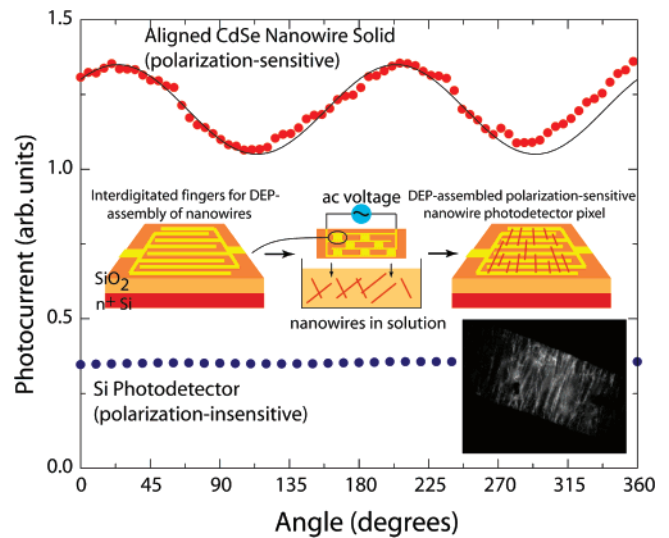
attractive feature. With the Fabry–Perot design demonstrated earlier in this work, the responsivity can be enhanced at particular wavelengths.

Photocurrent Polarization Anisotropy. For investigating the polarization-sensitivity of the photodetectors, the NWs were aligned using ac dielectrophoresis (DEP). This entails applying a low-frequency ($\sim$1 kHz) ac electric field, with field strengths on the order of 1–40 kV/cm to NW solutions, upon which the NWs align between prepatterned Au electrodes on Si substrates having typical source-drain separations of 20–40 μm (the process is shown schematically in Figure 6 and described in detail elsewhere).[47] The NWs align on a time scale of 1 min and the process can be monitored through either brightfield or epifluorescence measurements on an inverted optical microscope. The DEP alignment is followed by the same annealing procedure described earlier for drop-cast photodetectors. NW alignment can subsequently be verified by absorption/emission polar-ization anisotropy measurements. These experiments yield typical absorption (emission) polarization anisotropy values of 0.75.[29]

Polarization-sensitive photocurrent measurements are mea-sured for the DEP-aligned photodetectors using the same apparatus described earlier with the 488 nm excitation of the QTH lamp. The polarization of the incident light is controlled by passing the excitation through a linear polarizer followed by a λ/4 waveplate to generate circularly polarized light. For polarization anisotropy measurements, an additional linear polarizer is mounted on a computer controlled rotation stage, which, in turn, provides variable angle linearly polarized light.

Figure 6 shows results of these polarization-sensitive measurements. Specifically under variable angle linearly

polarized light, a harmonic photocurrent response is observed and can be fit to a $\cos^2 \varphi$ function where φ is the angle between the incident polarization and the NW axis. Resulting photocurrent polarization anisotropy achieved is in the range ~13%. These values are in good agreement with analogous absorption and emission polarization anisotropies recently measured from individual NWs as well as their ensembles.[47] The origin of this polarization sensitivity comes from potential dielectric contrast effects as well as from confinement-induced optical selection rules.[31−33] Both predict very large anisotropies given that the bulk of the absorption occurs when the polarization of the incident light is parallel to the NW growth axis. The lower than ideal value of polarization anisotropy observed here is attributed to a fraction of nanowires that are not aligned between the electrodes but bridge aligned wires at various angles and contribute to the photocurrent via interwire carrier hopping. For comparison, the polarization-insensitive photocurrent measured by replacing the DEP-aligned CdSe photodetector by the Si photodetector is shown in Figure 6.

The DEP-aligned NW photodetectors extends the family of polarization-sensitive photodetectors from single-NW devices to their ensemble counterparts, but with a simple device fabrication procedure, one that does not require the formation of contacts to single nanowires. Other techniques for aligning the wires in parallel, such as those based on microfluidic flow, can be used in place of the DEP technique demonstrated here. With further refinement in the alignment procedure and modification of the dielectric environment, a larger polarization anisotropy can be achieved. Such quantum-wire-solid-based detectors may prove to be an attractive alternative to the top-down fabrication approaches currently employed for achieving polarization sensitivity in epitaxially grown layered heterostructures.[48]

Conclusions. Solution-synthesized CdSe nanowire solids were shown to be suitable for the fabrication of photoconductive photodetectors. The photodetectors exhibit absorption edge slopes of 32 nm/decade, and responsivities approaching ~0.1 A/W at high bias voltages. Aligning the nanowires between electrodes using ac dielectrophoresis makes the photocurrent sensitive to the polarization of the incident light, and polarization anisotropies ~13% are observed. Recent advances in the solution synthesis of CdS ($E_g = 2.42$ eV), CdSe (1.75 eV), CdTe (1.50 eV), PbS (0.37 eV), and PbSe (0.26 eV) semiconducting nanowires that cover a wide range of bandgaps implies that by building upon the results presented in this work and by other groups, multispectral polarization-sensitive photodetectors on virtually any substrate are a distinct possibility.[38,41] Furthermore, advances in solution synthesis of long semiconductor nanowires that are assembled in a simple cost-effective manner (either self-assembled or dielectrophoretically or microfluidic assembled) into thin films may offer a viable alternative to thin-film organic semiconductors. They have the potential to compete with organic thin films in every aspect: through superior and well-controlled electronic and optical properties, by the possibility for exploitation of size quantization, and finally, in the cost effectiveness and ease of transferring quantum-wire-solid-based device technologies to virtually any substrate.

References

(1) Li, Y.; Qian, F.; Xing, J.; Lieber, C. M. *Mater. Today* **2006**, *9*, 18.
(2) Dragoman, M.; Dragoman, D. *Nanoelectronics − Principles and Devices*; Artech House: Boston, 2006.
(3) Xiang, J.; Lu, W.; Hu, Y.; Wu, Y.; Yan, H.; Lieber, C. M. *Nature* **2006**, *441*, 489.
(4) Wang, J.; Gudiksen, M. S.; Duan, X.; Cui, Y.; Lieber, C. M. *Science* **2001**, *293*, 1455.
(5) Pettersson, H.; Tragardh, J.; Persson, A. I.; Landin, L.; Hessman, D.; Samuelson, L. *Nano Lett.* **2006**, *6*, 229.
(6) Gu, Y.; Kwak, E. S.; Lensch, J. L.; Allen, J. E.; Odom, T. W.; Lauhon, L. J. *Appl. Phys. Lett.* **2005**, *87*, 043111.
(7) Wagner, R. S.; Ellis, W. C. *Appl. Phys. Lett.* **1964**, *4*, 89.
(8) Morales, A. M.; Lieber, C. M. *Science* **1998**, *279*, 208.
(9) Holmes, J. D.; Johnston, K. P.; Doty, R. C.; Korgel, B. A. *Science* **2000**, *287*, 1471; Davidson, F. M.; Schricker, A. D.; Wiacek, R. J.; Korgel, B. A. *Adv. Mater.* **2004**, *16*, 646.
(10) Trentler, T. J.; Hickman, K. M.; Goel, S. C.; Viano, A. M.; Gibbons, P. C.; Buhro, W. E. *Science* **1995**, *270*, 1791. Yu, H.; Buhro, W. E. *Adv. Mater.* **2003**, *15*, 416. Yu, H.; Li, J. B.; Loomis, R. A.; Wang, L. W.; Buhro, W. E. *Nature Mater.* **2003**, *2*, 517. Yu, H.; Loomis, R. A.; Gibbons, P. C.; Wang, L-W.; Buhro, W. E. *J. Am. Chem. Soc.* **2003**, *125*, 16168.
(11) Murray, C. B.; Norris, D. J.; Bawendi, M. G. *J. Am. Chem. Soc.* **1993**, *115*, 8706.
(12) Peng, Z. A.; Peng, X. *J. Am. Chem. Soc.* **2001**, *123*, 168.
(13) McDonald, S. A.; Konstantatos, G.; Zhang, S.; Cyr, P. W.; Klem, E. J. D.; Levina, L.; Sargent, E. H. *Nature Mat.* **2005**, *4*, 138.
(14) Oertel, D. C.; Bawendi, M. G.; Arango, A. C.; Bulovic, V. *Appl. Phys. Lett.* **2005**, *87*, 213505.
(15) Jarosz, M. V.; Porter, V. J.; Fisher, B. R.; Kastner, M. A.; Bawendi, M. G. *Phys. Rev. B* **2004**, *70*, 195327.
(16) Porter, V. J.; Mentzel, T.; Charpentier, S.; Kastner, M. A.; Bawendi, M. G. *Phys. Rev. B* **2006**, *73*, 155303.
(17) Katari, J. E. B.; Colvin, V.; Alivisatos, A. P. *J. Phys. Chem.* **1994**, *98*, 4109.
(18) Talapin, D. V.; Murray, C. B. *Science* **2005**, *310*, 86.
(19) Klimov, V. I., *J. Phys. Chem. B* **2000**, *104*, 6112−6123.
(20) Ricard, D.; Ghanassi, M.; Schanneklein, M. C. *Opt. Commun.* **1994**, *108*, 311−318.
(21) Leatherdale, C. A.; Woo, W. K.; Mikulec, F. V.; Bawendi, M. G. *J. Phys. Chem. B* **2002**, *106*, 7619.
(22) Yu, W. W.; Qu, L. H.; Guo, W. Z.; Peng, X. G. *Chem. Mater.* **2003**, *15*, 2854−2860.
(23) Yu, D.; Wang, C.; Wehrenberg, B. L.; Guyot-Sionnest, P. *Phys. Rev. Lett.* **2004**, *92*, 216802−1.
(24) Schaller, R. D.; Klimov, V. I. *Phys. Rev. Lett.* **2004**, *92*, 186601.
(25) Ellingson, R. J.; Beard, M. C.; Johnson, J. C.; Yu, P.; Micic, O. I.; Nozik, A. J.; Shabaev, A.; Efros, A. L. *Nano Lett.* **2005**, *5*, 865.
(26) Konstantatos, G.; Howard, I.; Fischer, A.; Hoogland, S.; Clifford, J.; Klem, E.; Levina, L.; Sargent, E. H. *Nature* **2006**, *442*, 180.

(27) Phillips, J.; Kamath, K.; Bhattacharya, P. *Appl. Phys. Lett.* **1998**, *72*, 2020.

(28) Yu, W. W.; Qu, L. H.; Guo, W. Z.; Peng, X. G., *Chem. Mater.* **2003**, *15*, 2854−2860.

(29) Protasenko, V.; Bacinello, D.; Kuno, M., *J. Phys. Chem. B* **2006**, *110*, 25322.

(30) Romera, H. E.; Drndic, M. *Phys. Rev. Lett.* **2004**, *92*, 216802.

(31) Muljarov, E. A.; Zhukov, E. A.; Dneprovskii, V. S.; Masumoto, Y. *Phys. Rev. B* **2000**, *62*, 7420.

(32) Keldysh, L. V. *Phys. Stat. Solidi* (*a*) **1997**, *164*, 3.

(33) Shabaev, A.; Efros, A. L. *Nano Lett.* **2004**, *4*, 1821.

(34) Klimov, V. I. *J. Phys. Chem. B* **2000**, *104*, 6112.

(35) Benisty, H.; Sotomayortorres, C. M.; Weisbuch, C. *Phys. Rev. B* **1991**, *44*, 10945.

(36) Robel, I.; Bunker, B. A.; Kamat, P. V.; Kuno, M. *Nano Lett.* **2006**, *6*, 1344.

(37) Mohamed, M. B.; Burda, C.; El-Sayed, M. A. *Nano Lett.* **2001**, *1*, 589.

(38) Kuno, M.; Ahmad, O.; Protasenko, V.; Bacinello, D.; Kosel, T. *J. Phys. Chem. B* **2006**, *18*, 5722.

(39) Grebinksi, J. W.; Richter, K. L.; Zhang, J.; Kosel, T. H.; Kuno, M. *J. Phys. Chem. B* **2004**, *108*, 9745.

(40) Grebinski, J. W.; Hull, K. L.; Zhang, J.; Kosel, T. H.; Kuno, M. *Chem. Mater*. **2004**, *16*, 5260.

(41) Hull, K. L.; Grebinski, J. W.; Kosel, T. H.; Kuno, M. *Chem. Mater.* **2005**, *17*, 4416.

(42) Protasenko, V. V.; Hull, K. L.; Kuno, M. *Adv. Mater.* **2005**, *17*, 2942.

(43) Khandelwal, A.; Jena, D.; Grebinski, J. W.; Hull, K. L.; Kuno, M. *J. Electron. Mater.* **2006**, *35*, 170.

(44) Fan, Z.; Chang, P-c.; Lu, J. G.; Walter, E. C.; Penner, R. M.; Lin, C-h.; Lee, P. H.; *Appl. Phys. Lett.* **2004**, *85*, 6128.

(45) Unlu, M. S.; Kishino, K.; Liaw, H. J.; Morkoc, H. *J. Appl. Phys.* **2007**, *101*, 073704.

(46) Moddel, G.; Anderson, D. A.; Paul, W. *Phys. Rev. B* **1980**, *22*, 1918.

(47) Zhou, R.; Chang, H-C.; Protasenko, V.; Kuno, M.; Singh, A. K.; Jena, D.; Xing, H. *J. Appl. Phys.* **2007**, *101*, 073704.

(48) Chen, C. J.; Choi, K. K.; Rokhinson, L.; Chang, W. H.; Tsui, D. C. *Appl. Phys. Lett.* **1999**, *74*, 862.